Electronic circular dichroism from real-time propagation in state space

M. Monti, M. Stener, and E. Coccia[a)]

AFFILIATIONS

Dipartimento di Scienze Chimiche e Farmaceutiche, Università di Trieste, Via L. Giorgieri 1, 34127 Trieste, Italy

[a)]**Author to whom correspondence should be addressed:** ecoccia@units.it

ABSTRACT

In this paper, we propose to compute the electronic circular dichroism (ECD) spectra of chiral molecules using a real-time propagation of the time-dependent Schrödinger equation (TDSE) in the space of electronic field-free eigenstates, by coupling TDSE with a given treatment of the electronic structure of the target. The time-dependent induced magnetic moment is used to compute the ECD spectrum from an explicit electric perturbation. The full matrix representing the transition magnetic moment in the space of electronic states is generated from that among pairs of molecular orbitals. In the present work, we show the ECD spectra of methyloxirane, of several conformers of L-alanine, and of the Λ-Co(acac)$_3$ complex, computed from a singly excited ansatz of time-dependent density functional theory eigenstates. The time-domain ECD spectra properly reproduce the frequency-domain ones obtained in the linear-response regime and quantitatively agree with the available experimental data. Moreover, the time-domain approach to ECD allows us to naturally go beyond the ground-state rotationally averaged ECD spectrum, which is the standard outcome of the linear-response theory, e.g., by computing the ECD spectra from electronic excited states.

I. INTRODUCTION

The electronic circular dichroism (ECD) is the absorption difference exhibited by enantiomers of chiral molecules when interacting with left- and right-circularly polarized light. The theoretical understanding of ECD has been widely reported in the literature over the years.[1–7] ECD is employed to assign the absolute configuration of chiral compounds.[8] One can compute the ECD spectrum by using the response of the time-dependent induced magnetic dipole to an electric-field perturbation or the response of the time-dependent electric dipole to a magnetic-field perturbation.

Plenty of theoretical developments to compute the ECD spectra of chiral molecules have been published over the years: wave-function methods,[9–13] such as the time-dependent Hartree–Fock[10,14] and coupled cluster,[10,15–18] and parameterized approaches, such as the semiempirical method[19] and tight-binding based on Tamm–Dancoff approximation.[20] Among the various electronic-structure approaches, the time-dependent density functional theory (TDDFT) has been extensively employed for ECD applications and method development.[6,10,21–38]

Most of these methods rely on frequency domain, while less effort has been devoted to time-domain methods.[21,23–25] Here, we propose an approach based on the propagation of the time-dependent Schrödinger equation (TDSE) in the presence of an explicit electromagnetic field, in length gauge.[39–46] The time-dependent wave function is expanded into the set of eigenstates of the field-free Hamiltonian, making the approach general and applicable, in principle, to any level of theory for the electronic structure.[47–61] The time evolution of the magnetic dipole moment is also computed in the basis of field-free eigenstates. Propagating TDSE in the state space allows us to decouple the electronic-structure treatment from how TDSE is propagated in time, at variance with the methods based on the dynamics in the space of molecular orbitals:[62–64] first, the field-free problem is solved using the chosen methodology, providing ingredients for TDSE such as eigenenergies and transition dipole moments; second, TDSE is propagated in the presence of an explicit pulse to simulate the desired electron dynamics. Details are given in Sec. II.

In the present work, we computed the ECD spectrum of (R)- and (S)-methyloxirane, of various conformers of L-alanine, and of the Λ-Co(acac)$_3$ complex (Fig. 1), using TDDFT eigenstates, formulated within a singly excited ansatz, for defining the propagation space. We first compared the real-time ECD spectra with those obtained by a standard frequency-domain linear response and then with the experimental data, when available. Moreover, we studied the linear absorption and ECD of excited methyloxirane, assum-

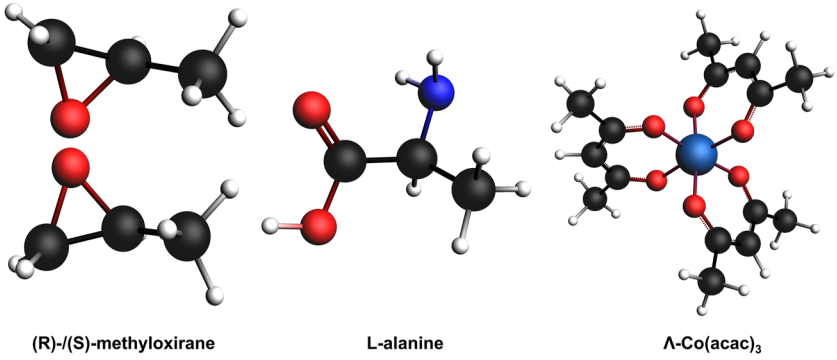

FIG. 1. Stick-and-ball representation of (R)-/(S)-methyloxirane, L-alanine, and Λ-Co(acac)$_3$. C, O, N, H, and Co atoms are reported in black, red, blue, white, and cobalt-blue, respectively.

ing as the initial condition of the propagation the molecule being in its first bright electronic excited state,[64] and analyzed the contribution to the ECD spectrum of Λ-Co(acac)$_3$ due to the different linear polarizations of the incoming pulse.

This article is organized as follows: in Sec. II, we present our method based on TDSE propagation; the computational details are given in Sec. III; the results are shown and discussed in Sec. IV; and then, the conclusions and perspectives are given in Sec. V.

II. THEORY

A. Time propagation

Here, we focus on the electric perturbation of the magnetic response of the system. TDSE in length gauge is given by (atomic units are used in this work)

$$i\frac{d}{dt}|\psi(t)\rangle = \hat{H}(t)|\psi(t)\rangle, \tag{1}$$

where $|\psi(t)\rangle$ is the time-dependent wave function and $\hat{H}(t)$ is the time-dependent Hamiltonian, which is composed of the field-free Hamiltonian $\hat{H}_0$ and the coupling between the molecular electric dipole operator $\vec{\hat{\mu}}$ and the external field $\vec{F}(t)$,

$$\hat{H}(t) = \hat{H}_0 - \vec{\hat{\mu}} \cdot \vec{F}(t). \tag{2}$$

$|\Psi(t)\rangle$ is practically expressed as a linear combination of the N_{states} field-free eigenstates (in this work, the DFT ground state and the $N_{\text{states}}-1$ TDDFT eigenstates) as

$$|\psi(t)\rangle = \sum_{M=0}^{N_{\text{states}}-1} C_M(t)|M\rangle. \tag{3}$$

Here, $C_M(t)$ are time-dependent coefficients and $|M\rangle$ is the Mth eigenstate of the system, with the eigenvalue E_M. In the space of such eigenstates, TDSE in Eq. (1) becomes

$$i\frac{\mathrm{d}\mathbf{C}(t)}{\mathrm{d}t} = \mathbf{H}(t)\mathbf{C}(t), \tag{4}$$

with $\mathbf{C}(t)$ being the vector of the expansion coefficients and $\mathbf{H}(t)$ being the matrix representation at time t of $\hat{H}(t)$, i.e., $(\mathbf{H}(t))_{LM} = \langle L|\hat{H}(t)|M\rangle$. The time-dependent Hamiltonian $\hat{H}(t)$ is diagonal for the field-free part of the eigenenergies E_M and characterized by the transition (electric) dipole moments $\langle L|\hat{\mu}|M\rangle$ between states,[44]

$$\langle L|\hat{H}(t)|M\rangle = E_M\delta_{LM} - \sum_\gamma F_\gamma(t)\langle L|\hat{\mu}_\gamma|M\rangle, \tag{5}$$

where $\gamma = x, y$, or z corresponds to the Cartesian component of the dipole and of the field. The numerical gauge-invariance for the ECD spectra has been previously tested and verified.[22] We use the TDDFT eigenvectors within a configuration-interaction singles ansatz[44,65] for the excited states,

$$|M\rangle = \sum_i^{occ}\sum_a^{vir} d^a_{i,M}|\Phi^a_i\rangle, \tag{6}$$

where $|\Phi^a_i\rangle$ is the singly excited Slater determinant, with an electron promoted from the occupied orbital i to the virtual one a, while $d^a_{i,M}$ are the amplitudes of the expansion for the state $|M\rangle$. Expansion coefficients, $d^a_{i,M}$, and the excited-state eigenenergies are computed by the Amsterdam Modeling Suite (AMS),[66] as reported in Sec. III.

B. Computing ECD spectrum

In order to compute the ECD spectrum in a large frequency range, we apply a kick pulse, modeled by a narrow Gaussian

$$\vec{F}(t) = \vec{F}_{\max}\exp\left(-\frac{(t-t_0)^2}{2\sigma^2}\right), \tag{7}$$

where $\vec{F}_{\max}$ is the field amplitude (the intensity I is equal to $\frac{1}{2}|\vec{F}_{\max}|^2$) and t_0 and σ are the center and the amplitude of the Gaussian, respectively.

The magnetic dipole moment operator $\vec{\hat{m}}$ is defined, neglecting the spin contribution, as[2]

$$\vec{\hat{m}} = -\frac{1}{2\,\mathrm{c}}\vec{\hat{r}} \times \vec{\hat{p}}, \tag{8}$$

with $\vec{\hat{r}}$ and $\vec{\hat{p}}$ being the position and momentum operators, respectively, and c being the light speed.

At each time t of the simulation, the induced magnetic dipole $\Delta\vec{m}(t)$ is defined as the difference between the time-dependent

magnetic moment $\vec{m}(t)$ at time t and that at initial time ($t = 0$), $\vec{m}(0)$,

$$\Delta\vec{m}(t) = \vec{m}(t) - \vec{m}(0). \tag{9}$$

Explicitly, $\vec{m}(t)$ and $\vec{m}(0)$ are computed from the TDSE propagation in state space,

$$\vec{m}(t) = \sum_{LM} C_L^*(t) C_M(t) \langle L|\vec{\hat{m}}|M\rangle, \tag{10}$$

$$\vec{m}(0) = \sum_{LM} C_L^*(0) C_M(0) \langle L|\vec{\hat{m}}|M\rangle. \tag{11}$$

The transition magnetic moment $\langle L|\vec{\hat{m}}|M\rangle$ can be expressed on the basis of Slater determinants. When one of the electronic states is the ground state $|0\rangle = |\Phi_0\rangle$ (with $|\Phi_0\rangle$ the DFT Slater determinant, in our specific case), one finds, using Eq. (6),

$$\langle L|\vec{\hat{m}}|0\rangle = \sum_{i}^{occ}\sum_{a}^{vir} d_{i,L}^{a} \langle \Phi_i^a|\vec{\hat{m}}|\Phi_0\rangle, \tag{12}$$

while the transition magnetic moment between two excited states is

$$\langle L|\vec{\hat{m}}|M\rangle = \sum_{i}^{occ}\sum_{a}^{vir}\sum_{j}^{occ}\sum_{b}^{vir} d_{i,L}^{a} d_{j,M}^{b} \langle \Phi_i^a|\vec{\hat{m}}|\Phi_j^b\rangle. \tag{13}$$

The generic transition magnetic moment $\langle \Phi_i^a|\vec{\hat{m}}|\Phi_j^b\rangle$ is, in turn, obtained by applying the Slater–Condon rules,[44]

$$\langle \Phi_i^a|\vec{\hat{m}}|\Phi_j^b\rangle = \begin{cases} \vec{M}_0 - \vec{m}_{ii} + \vec{m}_{aa}, & i = j, a = b, \\ \vec{m}_{ab}, & i = j, a \neq b, \\ -\vec{m}_{ji}, & i \neq j, a = b, \\ 0, & i \neq j, a \neq b, \end{cases} \tag{14}$$

where $\vec{M}_0 = \langle \Phi_0|\vec{\hat{m}}|\Phi_0\rangle = \sum_i \vec{m}_{ii}$ and the generic $\vec{m}_{st}$ is the magnetic moment matrix element in the molecular-orbital (MO) representation. In practice, AMS explicitly computes the transition matrix elements in the MO space, which are then transformed into $\langle \Phi_i^a|\vec{\hat{m}}|\Phi_j^b\rangle$ and into $\langle L|\vec{\hat{m}}|M\rangle$ by means of an interface between AMS and WaveT, which accounts for the antisymmetric nature of the magnetic matrix. The ECD spectrum is finally computed as the imaginary part of the following:

$$P_{nl}^{ECD}(\omega) = -\frac{i}{2\pi\omega F_n^0(\omega)} \int_0^{+\infty} -\Delta m_l(t) e^{i(\omega+i\Gamma)t} dt. \tag{15}$$

In Eq. (15), $F_n^0(\omega)$ is the Fourier transform of the component n of the external field, $\Delta m_l(t)$ is the component l of the induced magnetic dipole, and Γ is a damping parameter reproducing an exponential decay of the excited-state population.[22] The comparison with the experimental spectra is performed using a rotational average, i.e.,

$$\bar{P}^{ECD}(\omega) = \frac{1}{3}\left(P_{xx}^{ECD}(\omega) + P_{yy}^{ECD}(\omega) + P_{zz}^{ECD}(\omega)\right). \tag{16}$$

III. COMPUTATIONAL DETAILS

The ground-state geometries of the (S)-methyloxirane and Λ-Co(acac)$_3$ system have been optimized at the DFT level[67] by the Amsterdam Density Functional (ADF) engine[68] of the AMS code.[66] Both the optimizations were realized using the hybrid B3LYP[69] exchange-correlation (xc) functional and a triple-zeta plus polarization TZP basis set of Slater-type orbitals. The geometry of the (R)-methyloxirane has been obtained by inverting the x coordinates of the optimized S enantiomer. For the L-alanine, we have considered seven low-energy conformers, taking both the relative energies and the geometry structures, optimized at the df-CCSD(T)-F level with the aug-cc-pVDZ-F12 basis set, from a recent study.[70] For all the systems, we have then calculated the ECD spectra in the frequency domain at the time-dependent DFT (TDDFT) level by using the Casida approach.[71] The eigenvalue problem is solved by means of the Davidson algorithm. We have extracted the lowest 20, 40, and 100 excited-states for the methyloxirane, L-alanine, and Λ-Co(acac)$_3$, respectively. These choices have been made in order to cover the experimental frequency range. The ECD calculations have been performed using the B3LYP and the long-range corrected CAM-B3LYP[72] functionals. Moreover, for the L-alanine, we have tested the range-separated wB97X-D functional, which includes the dispersion and non-local exchange corrections, allowing a proper treatment of the amino acid intra-molecular H bonds.[32,73] All the ECD spectra have been calculated in gas phase. For the Λ-Co(acac)$_3$ complex, we have additionally performed the ECD calculation, simulating the solvent (ethanol) effect with the conductor like screening model (COSMO) of solvation[74] available in AMS. Finally, all the ECD spectra have been convoluted by using Gaussian functions with a half width at half maximum (HWHM) equal to 0.15 eV.

The time-domain ECD calculations have been performed with the in-house WaveT package,[43] whose interface with AMS has been recently proposed for the electric transition dipole moment[44] and here extended for the magnetic transition dipole moment, as explained in Sec. II. In practice, excitation energies and transition dipole moments (both electric and magnetic, after the transformation performed by the interface) are provided by the TDDFT calculations and then employed as input parameters for the real-time propagation. For all the systems in Fig. 1, 250-fs dynamics have been simulated with a time step δt of 0.12×10^{-2} fs. Different values of time length (100, 150, 250, and 300 fs) and time step (0.12×10^{-2}, 0.24×10^{-2}, and 0.24×10^{-3} fs) have been tested to ensure the convergence of the dynamics. The results of these convergence tests are shown in Figs. S1 and S2 of the supplementary material. The time-dependent external field [see Eq. (7)] has been reproduced with a kick pulse of 10^5 W/cm^2 intensity and a full width at half maximum of 0.094 fs for the Gaussian envelope. The value of the damping parameter Γ in Eq. (15) is 5 fs for all the cases. The ECD spectrum in Eq. (15) has been computed with a post-processing tool implemented in WaveT, using the TDSE dynamics as input. The final spectra have been obtained averaging the results, according to Eq. (16).

For all the cases, the energy range of both frequency- and time-domain ECD calculations has been adapted to the experimental one (i.e., eV, nm, and cm^{-1}) for a suitable comparison of the results.

IV. RESULTS AND DISCUSSION

This section is organized as follows: for each molecule in Fig. 1, we first compare the time-domain ECD spectra [i.e., obtained by Eqs. (15) and (16)] with the standard frequency-domain ones and

then with the experimental data available in the literature,[70,75,76] using the units of the original works. Additional analyses on the excited-state absorption, the role of the solvent in ECD, and the interplay between the $\vec{F}$ polarization and magnetic transition dipole moment are reported for *S*-methyloxirane and Λ-Co(acac)$_3$ in the corresponding subsections.

A. (R)- and (S)-methyloxirane

The ECD spectra obtained with AMS (frequency domain) and WaveT (time domain), using the B3LYP functional, reveal an almost perfect overlap for both the enantiomers of the methyloxirane, as shown in Fig. 2: the shape and relative intensities of the peaks are conserved moving from a frequency to a real-time calculation. The small discrepancies could be due to the different smoothing techniques applied. These results clearly show that the interface between the two codes produces the right transition magnetic moments in the state space of Eqs. (12) and (13) and, in turn, that WaveT computes the right temporal evolution of the magnetic transition dipole moment. Considering the CAM-B3LYP functional (see Fig. S3 of the supplementary material), we still find a good agreement between the frequency-domain and time-domain calculations, with only the small discrepancies that can be associated again with the smoothing strategy. We can also notice that the overall ECD pattern calculated with CAM-B3LYP resembles that obtained with the B3LYP functional, although blueshifted by around 0.6 eV and with some differences in terms of the intensity ratio of the peaks. As a matter of fact, such discrepancies make the agreement between the CAM-B3LYP calculations and the experimental spectra less accurate (Fig. S4 of the supplementary material). Therefore, from here on, we will only consider the real-time calculations carried out with B3LYP for the comparison with the experimental ECD.

We can notice in Fig. 3 an overall good agreement between the experimental ECD spectra measured in the gas-phase[75] and our time-domain ECD propagated in vacuum, with the discrepancies being more marked for the (S)-methyloxirane. Indeed, the experimental positive feature located at 7.20 eV is slightly redshifted in the calculation and the same goes for the following peak, whose experimental negative maximum is found at around 7.80 eV. In addition to that, the calculated peaks from 8.5 eV onward show

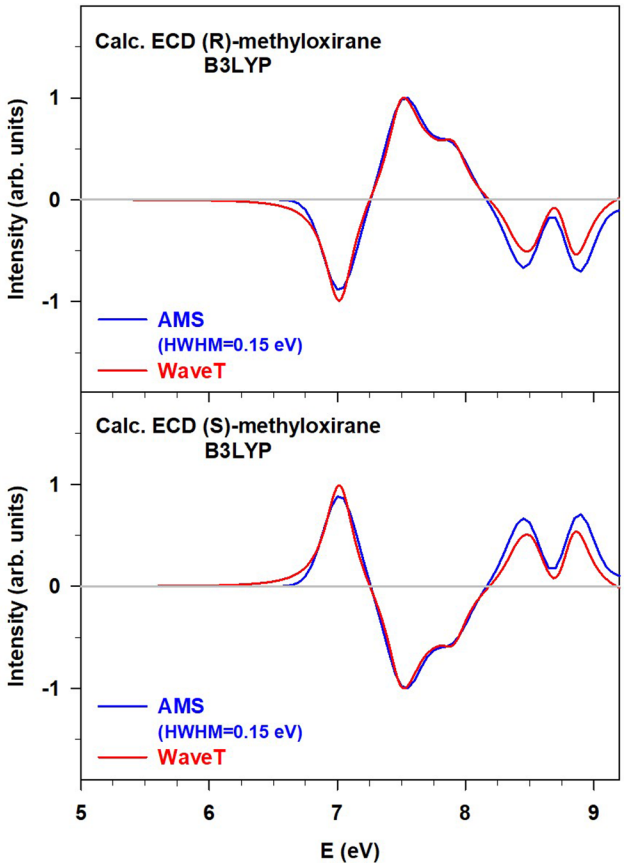

FIG. 2. Comparison of the ECD spectra calculated for (R)-methyloxirane (top panel) and (S)-methyloxirane (bottom panel) using the B3LYP functional and the AMS (frequency-domain, solid blue line) and the WaveT (time-domain, solid red line) code. All the intensities have been normalized and reported in arbitrary units (arb. units).

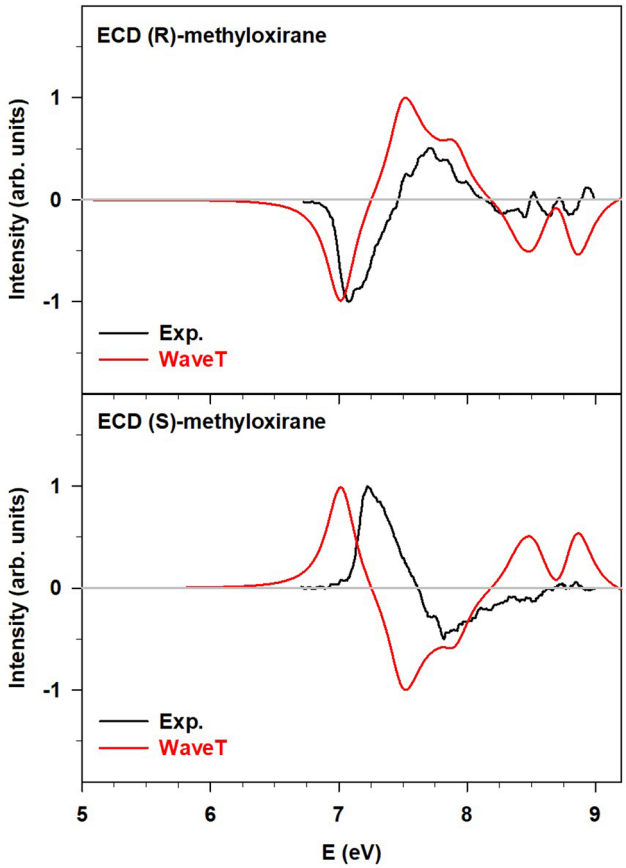

FIG. 3. Comparison between the experimental (solid black line)[75] and real-time calculated (solid red line) (B3LYP functional) ECD spectra of (R)-methyloxirane (top panel) and (S)-methyloxirane (bottom panel). All the intensities have been normalized and reported in arbitrary units (arb. units).

a higher intensity with respect to the corresponding experimental ones. Nevertheless, most of the discrepancies are reconciled, noticing that while the calculated features of the two enantiomers have equal and opposite signs, the experimental patterns slightly deviate from being mirror images. Therefore, considering this experimental limitation, both the calculations properly reproduce all the main features of the system.

Besides checking the implementation, we also calculated the absorption and ECD spectra of (S)-methyloxirane from the first (bright) excited state. For computing the optical properties from ground state, the initial condition in the electron dynamics is given by $|C_0(t=0)|^2 = 1$; see Eq. (3). For a generic $|M\rangle$ state, with $M > 0$, running an excited-state dynamics corresponds to $|C_M(t=0)|^2 = 1$. In our case, $M = 1$. The simulation was run on the ground state geometry, thus simulating a vertical excitation. This scheme resembles a pump–probe experiment, where the delay time between the two pulses is small enough to measure the observable of interest without changing the geometry of the system. Indeed, time-resolved circular dichroism spectroscopy has recently become a powerful experimental tool to study the dynamics in chiral molecular systems.[77–82] The influence of the electronic state on the optical response is well highlighted in Fig. 4, where significant changes have been found populating the first excited state for both the absorption and ECD spectra. Indeed, looking at the top panel of Fig. 4, we observe that the ground state absorption peaks, located in the vacuum-UV region, are drastically shifted toward the near-IR/visible energy range when the system is excited. Furthermore, the inset in the top panel of Fig. 4 reveals the presence of the absorption and emission peaks involving the $|0\rangle$ and the $|1\rangle$ states, both located at 7 eV. A significant change in the intensity scale is also noticed, with a strong $|0\rangle \rightarrow |3\rangle$ transition of absorption (i.e., peak A′ in Fig. 4, and Table I). Additional details on the principal transitions of both the absorption spectra are reported in Table I. The chiral features of the (S)-methyloxirane are also markedly dependent on the electronic state, as shown in the bottom panels of Fig. 4. In this case, the optical response in the vacuum-UV range is still observable for the first excited state, even though the main feature lies between (0–2) eV, but the pattern is diametrically opposite with respect to the ground-state one. Indeed, focusing on the peak centered at ~7 eV, where the $|1\rangle \rightarrow |0\rangle$ emission peak is observed (see above), it can be suggested that an ECD inversion occurs when the system is excited. A similar spectrum for the first-excited state has been recently reported by

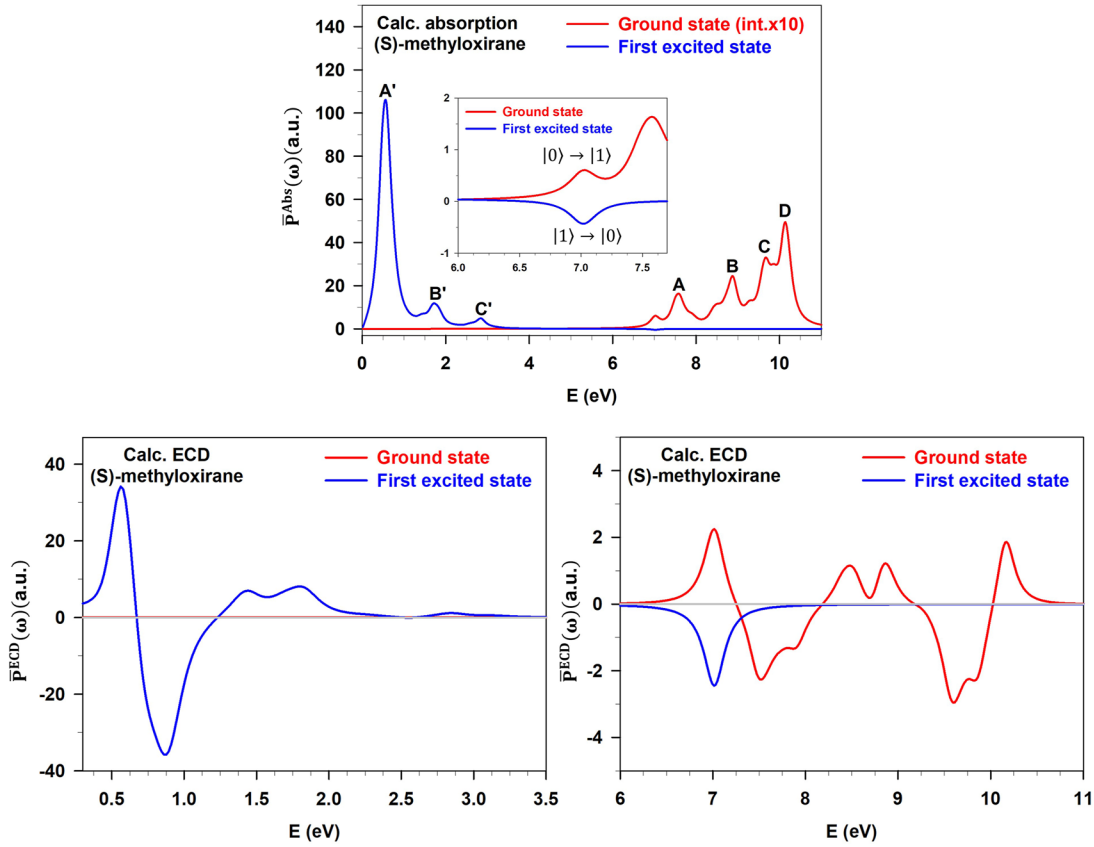

FIG. 4. Calculated (Calc.) absorption (top panel) and ECD (bottom panels) spectra of (S)-methyloxirane considering the ground state (solid red lines) and the first excited state (solid blue lines). In the inset of the top panel, the region between 6.0 and 7.7 eV has been highlighted to show the absorption and emission peaks involving the $|0\rangle$ and $|1\rangle$ states. Details of the significant absorption transitions are reported in Table I. Lower panels represent the same ECD spectrum up to 3.5 eV (left) and between 6 and 11 eV (right), with different vertical scales. No ECD signal is present between 3.5 and 6 eV. Intensities are in atomic units.

TABLE I. Transition and excitation energy for each significant peak of absorption of (S)-methyloxirane considering both the ground state and the first excited state.

Label	Transition	Excitation energy (eV)
A	$\|0\rangle \rightarrow \|3\rangle$	7.58
B	$\|0\rangle \rightarrow \|11\rangle$	8.87
C	$\|0\rangle \rightarrow \|15\rangle$	9.68
D	$\|0\rangle \rightarrow \|17\rangle$	10.11
A′	$\|1\rangle \rightarrow \|3\rangle$	0.56
B′	$\|1\rangle \rightarrow \|9\rangle$	1.72
C′	$\|1\rangle \rightarrow \|16\rangle$	2.83

Andersen and co-workers,[18] even though only the 0–2 eV range is shown in that work.

B. L-alanine

For L-alanine, we compared the frequency-domain and time-domain ECD spectra considering the B3LYP, CAM-B3LYP, and wB97X-D xc functionals, as explained in detail in Sec. III and as shown in Fig. 5. We have used the most stable conformer of the amino acid, as reported in Ref. 70. All the results support the consistency between the Casida and real-time calculations. Differences arise in the ECD spectrum according to the chosen xc functional. For instance, after redshifting the frequency-domain and time-domain wB97X-D spectra by 10 nm, we can notice two distinguishable positive peaks in the 140–160 nm energy range, while only a single positive feature is centered at around 145/150 nm for the B3LYP/CAM-B3LYP ECD spectra, respectively. From 170 nm onward, some similarities for the features calculated with the range-separated functionals (CAM-B3LYP and wB97X-D) are found, although they differ in terms of intensity values, while the response is less defined with B3LYP. Since the calculation performed with the wB97X-D shows closer resemblances with the experimental spectrum (as it will be shown below), consistently with the data available in the literature for amino acids and peptides,[32,73] it will be the only one considered from here on for L-alanine.

Before comparing the experimental and calculated spectra, it is worth emphasizing the high sensitivity of the ECD toward conformational changes. This aspect becomes particularly relevant when a flexible system, e.g., an amino acid, is treated, since a significant number of conformations will contribute to the overall optical response. Therefore, a balance must be found between the inclusion of, at least, the low-energy conformations and the computational effort, which increases proportionally to the number of structures considered. The conformational investigation of the gas-phase alanine has been carried out in several studies,[83,84] including the recent work of Meinert *et al.*,[70] where seven stable conformers have been extracted and used in the ECD calculations. Starting from these available data, we have calculated a statistically weighted ECD at 300 K and then compared with the experimental response and the calculated spectrum for the most probable conformation (as already shown in Fig. 5). All the results are collected in Fig. 6, while details on the conformers are reported in Table S1 of the supplementary material. We can notice that the experimental features are well reproduced by both the redshifted computed spectra, with only some

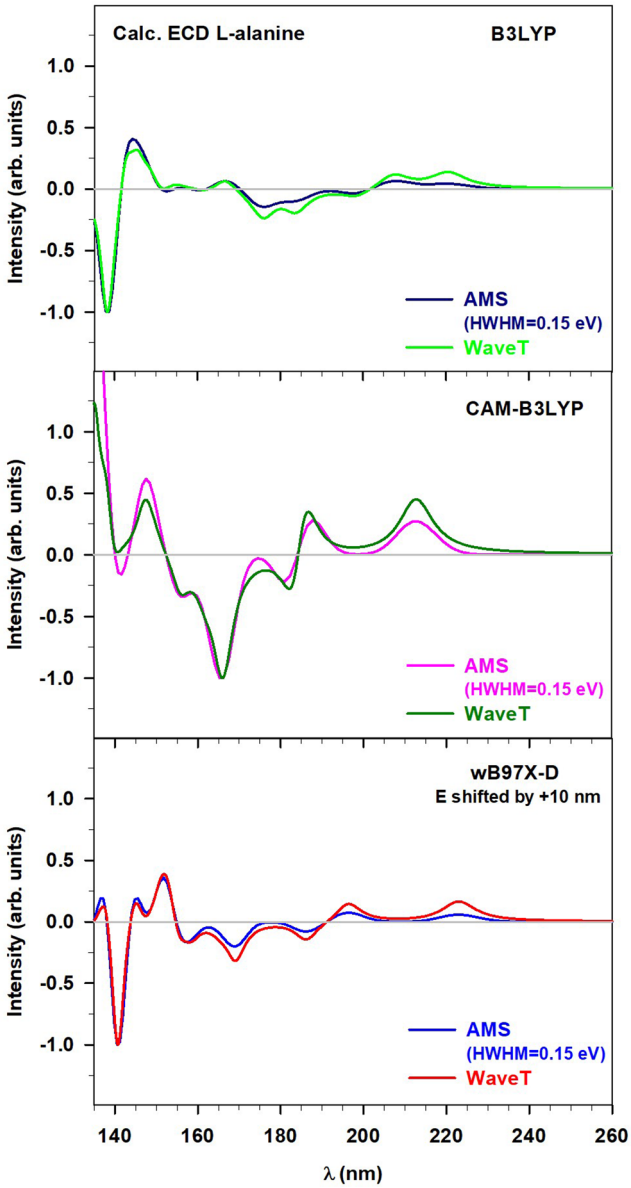

FIG. 5. Comparison of the ECD spectra calculated with AMS (frequency-domain) and WaveT (time-domain) for L-alanine. The B3LYP (top panel), CAM-B3LYP (middle panel), and wB97X-D (bottom panel) xc functionals have been used. The ECD spectra calculated with the wB97X-D functional have been redshifted by +10 nm. All the intensities have been normalized and reported in arbitrary units (arb. units).

differences in the intensity around 180 nm. Figure 6 also reveals strong similarities between the statistical approach and the inclusion of only the most probable conformer, but they are justified considering the energy and probability values reported in Table S1 of the supplementary material. Indeed, since the lowest energy conformer is much more stable with respect to the other structures, its optical response becomes predominant in the averaged ECD spectrum. However, the individual time-domain ECD spectra reported in

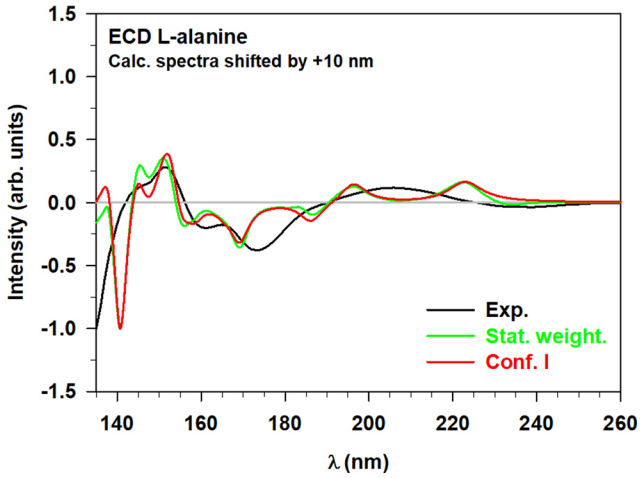

FIG. 6. Comparison between the experimental (solid black line)[70] and real-time calculated (wB97X-D functional) ECD spectra of L-alanine. The spectrum calculated statistically weighting the seven lowest energy conformations (solid green line) is reported together with that calculated considering only the most probable conformation (solid red line). All the intensities have been normalized and reported in arbitrary units (arb. units).

Fig. S5 of the supplementary material confirm the significant interplay between conformations and chirality.

C. Λ-Co(acac)$_3$

Also for the Λ-Co(acac)$_3$ complex, we started from the comparison between the frequency-domain and time-domain spectra, which confirms the good quality agreement between the AMS and WaveT results obtained employing the B3LYP functional, as shown in Fig. 7. Indeed, despite the small differences in intensity, particularly focused around 17×10^3 and 35×10^3 cm^{-1}, the Casida and real-time calculations match properly. The same comment can be applied to the CAM-B3LYP results (see the top panel of Fig. S6 of the supplementary material), with only small discrepancies in terms of intensity, particularly in the high energy range, between the frequency-domain and time-domain data. The CAM-B3LYP spectrum is blueshifted with respect to the B3LYP one. In addition to that, the intensity ratio of the two positive features centered at 37×10^3 and 41×10^3 cm^{-1}, respectively, in the B3LYP spectra is inverted in the CAM-B3LYP ones. Such differences lead to a worse agreement with the experimental ECD for the real-time calculation with CAM-B3LYP (Fig. S6 of the supplementary material, bottom panel); thus, only the B3LYP results will be discussed from here on.

The overall quality agreement is also observable comparing the experimental spectrum[76] with the real-time propagation (Fig. 8), which, hence, reproduces the main chiroptical properties of the Λ-Co(acac)$_3$, despite some energy and intensity discrepancies. Indeed, the experimental negative peaks centered at 31×10^3 and 45×10^3 cm^{-1}, respectively, find the theoretical correspondence in the peaks located at around 34×10^3 and 46×10^3 cm^{-1}, with the first calculated one exceeding in intensity. Instead, the positive features at ~17×10^3 and 39×10^3 cm^{-1} are properly reproduced by the small and double peak at around 19×10^3 and 40×10^3 cm^{-1}, respectively. It is worth noting that some limitations arise from the difference in the environment, since the experimental ECD has been measured in ethanol, while our dynamics is realized in vacuum (Fig. 8).

Therefore, we partially investigated the solvent role propagating the time-dependent wave function expanded in the TDDFT eigenstates equilibrated with an implicit description of ethanol at the AMS level and then propagated in vacuum. The corresponding result calculations are reported together with the experimental findings and the gas-phase ECD in Fig. 9. We can notice that even the partial treatment of the solvent provides a better description,

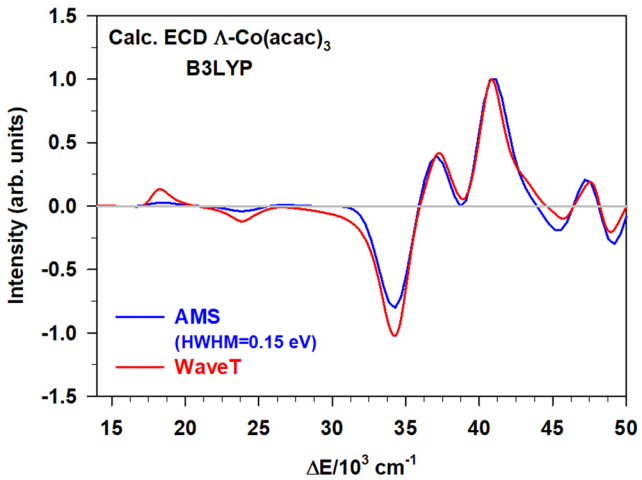

FIG. 7. Comparison of the ECD spectra calculated with AMS (frequency-domain, solid blue line) and WaveT (time-domain, solid red line) for the Λ-Co(acac)$_3$ complex. All the intensities have been normalized and reported in arbitrary units (arb. units).

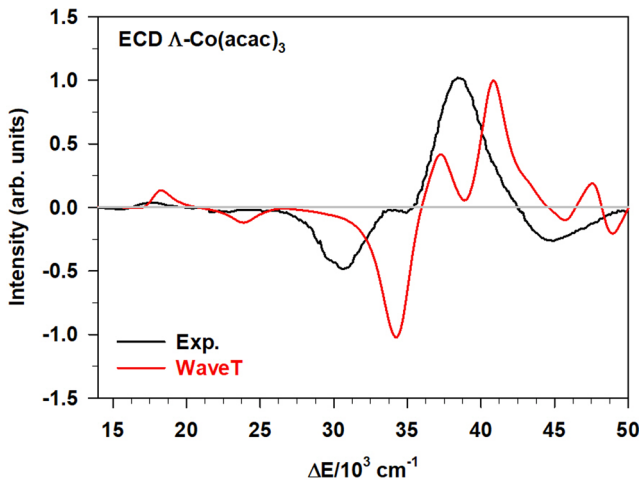

FIG. 8. Comparison between the experimental (solid black line)[76] and real-time calculated (solid red line) ECD spectra of the Λ-Co(acac)$_3$ complex. All the intensities have been normalized and reported in arbitrary units (arb. units).

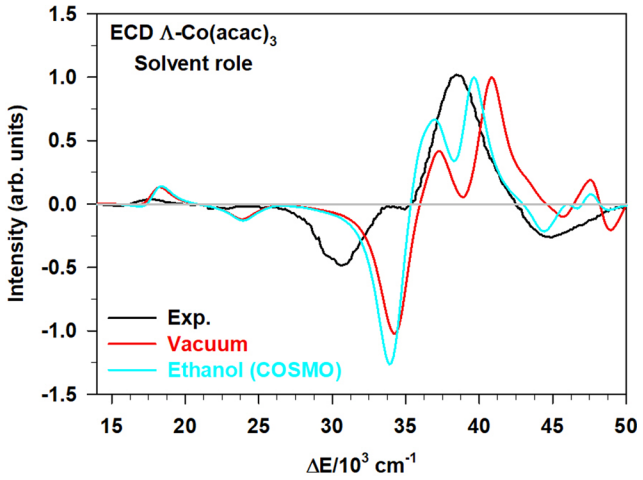

FIG. 9. The experimental ECD (solid black line)[76] spectrum of the Λ-Co(acac)$_3$ complex is reported together with the real-time ECD calculated in the gas phase (solid red line) and ethanol (solid cyan line), respectively. The solvent has been implicitly treated with the COSMO model available in AMS. All the intensities have been normalized and reported in arbitrary units (arb. units).

particularly in the 35–45 $\times 10^3$ cm^{-1} energy range where the double peak is well aligned with the corresponding experimental feature.

It is worth noting that a previous theoretical study on the same Co complex[85] furnished an ECD spectrum in satisfactory agreement with respect to the experiment,[76] despite an energy shift of 4×10^3 cm^{-1}. Considering that our calculations have not been shifted, the agreement of the present results is slightly better than the previous ones, with especially the features at 17×10^3 and 39×10^3 cm^{-1} improved by theory. Such an improvement should be ascribed to the more accurate hybrid exchange-correlation functional, which performs better than the GGA-BP86 functional used by Fan and Ziegler.[85]

We concluded our investigation on the Λ-Co(acac)$_3$ complex analyzing how each polarization direction of the external field $\vec{F}$ influences the temporal evolution of the corresponding component of the magnetic transition dipole moment and, thus, the ECD. Indeed, while the spectrum is usually shown, or directly obtained, as averaged on the three components, the contributions can be decomposed in the WaveT package since they are calculated independently. Considering, in particular, the Λ-Co(acac)$_3$ with its D_3 symmetry (see the left panel of Fig. 10), it is interesting to perform a directional analysis. The ECD spectra reported in Fig. 10 (right panel) confirm the ability of our calculations to discriminate among the components, with the magnetic response to F_z along z different from those to F_x and F_y along x and y, respectively.

V. CONCLUSIONS

We have implemented an explicit interface between the AMS and WaveT codes in order to propagate the magnetic moment in the space of the electronic states. In this way, we have defined a general approach to compute the ECD spectra via TDSE, using the magnetic response to an electric perturbation.

We have applied this scheme to the (R)-/(S)-methyloxirane, L-alanine, and Λ-Co(acac)$_3$ chiral systems to validate its correct functioning. The frequency-domain (AMS) and time-domain (WaveT) ECD calculations are in excellent agreement, hence confirming the correct simulation of the temporal evolution of the magnetic transition dipole moment. Furthermore, for each system, the comparison between the real-time ECD spectra and the experimental data shows the good overall quality of our calculations, which all reproduce the main spectral features. Instead, for the cobalt complex, the differences between the experimental ECD, measured in an ethanol solution, and our propagation in vacuum can be related to the environmental conditions. This hypothesis has been corroborated with the static inclusion of the solvent in the wave function

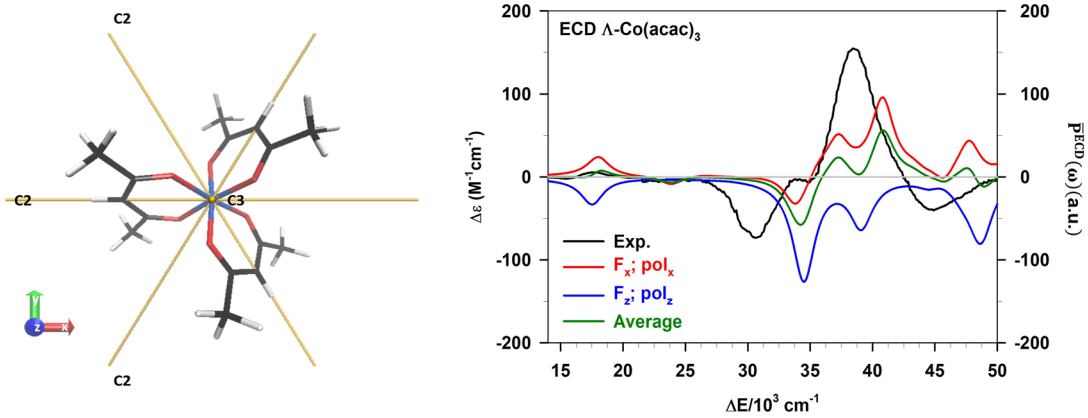

FIG. 10. Left panel: schematic representation of the D_3 symmetry of the Λ-Co(acac)$_3$ complex with the C_3 axis coincident with the z axis. Right panel: the experimental ECD (solid black line) spectrum of the Λ-Co(acac)$_3$ complex is reported together with those simulated considering the x (solid red line) and z (solid blue line) directions of the external field $\vec{F}$, respectively, and the real-time ECD averaged on the three components (solid dark green line). The experimental and calculated spectra are reported in M^{-1} cm^{-1} and atomic units (a.u.), respectively, without any normalization.

time evolution, which provides a better agreement between the experimental and time-domain ECD. In addition to this successful validation, we have investigated the excited state spectra and the relation between the $\vec{F}$ polarization and the ECD response. Propagating the wave packet of (S)-methyloxirane in its first excited state but with the ground state geometry, we have pointed out the significant changes that occur in the optical response following the system excitation. Indeed, while the absorption spectrum is entirely shifted toward the near IR/vis range, the ECD one reveals a sign inversion. For the symmetric Λ-$Co(acac)_3$, instead, we have decomposed the rotationally averaged ECD in its components, highlighting the optical changes in response to a different polarization of the external field.

ACKNOWLEDGMENTS

The authors acknowledge the computational support from the University of Trieste. E.C. acknowledges the funding from the University of Trieste under Grant No. MICROGRANTS 2020. The authors also thank S. Corni for inspiring suggestions. Financial support from ICSC – Centro Nazionale di Ricerca in High Performance Computing, Big Data and Quantum Computing, funded by European Union – NextGenerationEU is gratefully acknowledged.

AUTHOR DECLARATIONS

Conflict of Interest

The authors have no conflicts to disclose.

Author Contributions

M. Monti: Formal analysis (equal); Investigation (equal); Validation (equal); Writing – original draft (equal); Writing – review & editing (equal). **M. Stener**: Writing – review & editing (equal). **E. Coccia**: Conceptualization (lead); Investigation (lead); Methodology (lead); Supervision (lead); Writing – original draft (equal); Writing – review & editing (equal).

DATA AVAILABILITY

The data that support the findings of this study are available from the corresponding author upon reasonable request.

REFERENCES

[1] P. Lazzeretti, Adv. Chem. Phys. **75**, 507 (1989).
[2] P. Lazzeretti, *Handbook of Molecular Physics and Quantum Chemistry* (Wiley, 2003), Vol. 3, p. 53.
[3] C. Diedrich and S. Grimme, J. Phys. Chem. A **107**, 2524 (2003).
[4] T. D. Crawford, Theor. Chem. Acc. **115**, 227 (2006).
[5] T. D. Crawford, M. C. Tam, and M. L. Abrams, J. Phys. Chem. A **111**, 12057 (2007).
[6] I. Warnke and F. Furche, Wiley Interdiscip. Rev.: Comput. Mol. Sci. **2**, 150 (2012).
[7] S. S. Andrews and J. Tretton, J. Chem. Educ. **97**, 4370 (2020).
[8] N. Berova, L. D. Bari, and G. Pescitelli, Chem. Soc. Rev. **36**, 914 (2007).
[9] M. Scott, D. R. Rehn, P. Norman, and A. Dreuw, J. Phys. Chem. Lett. **12**, 5132 (2021).
[10] N. Niemeyer, M. Caricato, and J. Neugebauer, J. Chem. Phys. **156**, 154114 (2022).
[11] D. M. Rogers, H. Do, and J. D. Hirst, Mol. Phys. **120**, e2133748 (2022).
[12] M. Schreiber, R. Vahrenhorst, V. Buss, and M. P. Fülscher, Chirality **13**, 571 (2001).
[13] F. Gendron, B. Moore II, O. Cador, F. Pointillart, J. Autschbach, and B. Le Guennic, J. Chem. Theory Comput. **15**, 4140 (2019).
[14] A. E. Hansen and T. D. Bouman, J. Am. Chem. Soc. **107**, 4828 (1985).
[15] T. B. Pedersen, H. Koch, and K. Ruud, J. Chem. Phys. **110**, 2883 (1999).
[16] J. Kongsted, T. B. Pedersen, A. Osted, A. E. Hansen, K. V. Mikkelsen, and O. Christiansen, J. Phys. Chem. A **108**, 3632 (2004).
[17] D. A. Fedotov, S. Coriani, and C. Hättig, J. Chem. Phys. **154**, 124110 (2021).
[18] J. H. Andersen, K. D. Nanda, A. I. Krylov, and S. Coriani, J. Chem. Theory Comput. **18**, 1748 (2022).
[19] G. Bringmann, K.-P. Gulden, B. Holger, J. Fleischhauer, B. Kramer, and E. Zobel, Tetrahedron **49**, 3305 (1993).
[20] S. Grimme and C. Bannwarth, J. Chem. Phys. **145**, 054103 (2016).
[21] D. Varsano, L. A. Espinosa-Leal, X. Andrade, M. A. L. Marques, R. di Felice, and A. Rubio, Phys. Chem. Chem. Phys. **11**, 4481 (2009).
[22] S. Pipolo, S. Corni, and R. Cammi, Comput. Theor. Chem. **1040-1041**, 112 (2014).
[23] J. J. Goings and X. Li, J. Chem. Phys. **144**, 234102 (2016).
[24] J. Mattiat and S. Luber, Chem. Phys. **527**, 110464 (2019).
[25] J. Mattiat and S. Luber, J. Chem. Theory Comput. **18**, 5513 (2022).
[26] L. Konecny, M. Kadek, S. Komorovsky, K. Ruud, and M. Repisky, J. Chem. Phys. **149**, 204104 (2018).
[27] E. Makkonen, T. P. Rossi, A. H. Larsen, O. Lopez-Acevedo, P. Rinke, M. Kuisma, and X. Chen, J. Chem. Phys. **154**, 114102 (2021).
[28] W. D. Liu, J. Q. Wang, S. F. Yuan, X. Chen, and Q. M. Wang, Angew. Chem., Int. Ed. Engl. **60**, 11430 (2021).
[29] O. Baseggio, D. Toffoli, G. Fronzoni, M. Stener, L. Sementa, and A. Fortunelli, J. Phys. Chem. C **120**, 24335 (2016).
[30] L. Chang, O. Baseggio, L. Sementa, D. Cheng, G. Fronzoni, D. Toffoli, E. Aprà, M. Stener, and A. Fortunelli, J. Chem. Theory Comput. **14**, 3703 (2018).
[31] D. Toffoli, A. Russi, G. Fronzoni, E. Coccia, M. Stener, L. Sementa, and A. Fortunelli, J. Phys. Chem. Lett. **12**, 5829 (2021).
[32] M. Monti, M. Stener, and M. Aschi, J. Comput. Chem. **43**, 2023 (2022).
[33] D. Toffoli, M. Medves, G. Fronzoni, E. Coccia, M. Stener, L. Sementa, and A. Fortunelli, Molecules **27**, 93 (2022).
[34] H. Jang, N. J. Kim, and J. Heo, Comput. Theor. Chem. **1125**, 63 (2018).
[35] E. Molteni, G. Onida, and G. Tiana, J. Phys. Chem. B **119**, 4803 (2015).
[36] J. Autschbach, T. Ziegler, S. J. A. van Gisbergen, and E. J. Baerends, J. Chem. Phys. **116**, 6930 (2002).
[37] J. Autschbach and T. Ziegler, J. Chem. Phys. **116**, 891 (2002).
[38] J. Autschbach, S. Patchkovskii, T. Ziegler, S. J. A. van Gisbergen, and E. J. Baerends, J. Chem. Phys. **117**, 581 (2002).
[39] S. Pipolo and S. Corni, J. Phys. Chem. C **120**, 28774 (2016).
[40] E. Coccia, J. Fregoni, C. A. Guido, M. Marsili, S. Pipolo, and S. Corni, J. Chem. Phys. **153**, 200901 (2020).
[41] E. Coccia, F. Troiani, and S. Corni, J. Chem. Phys. **148**, 204112 (2018).
[42] E. Coccia and S. Corni, J. Chem. Phys. **151**, 044703 (2019).
[43] E. Coccia, Mol. Phys. **118**, e1769871 (2020).
[44] P. Grobas Illobre, M. Marsili, S. Corni, M. Stener, D. Toffoli, and E. Coccia, J. Chem. Theory Comput. **17**, 6314 (2021).
[45] G. Dall'Osto, E. Coccia, C. A. Guido, and S. Corni, Phys. Chem. Chem. Phys. **22**, 16734 (2020).

[46] G. Dall'Osto and S. Corni, J. Phys. Chem. A **126**, 8088 (2022).
[47] J. C. Tremblay, T. Klamroth, and P. Saalfrank, J. Chem. Phys. **129**, 084302 (2008).
[48] J. C. Tremblay, S. Klinkusch, T. Klamroth, and P. Saalfrank, J. Chem. Phys. **134**, 044311 (2011).
[49] P. Saalfrank, F. Bedurke, C. Heide, T. Klamroth, S. Klinkusch, P. Krause, M. Nest, and J. C. Tremblay, Adv. Quantum Chem. **81**, 15 (2020).
[50] F. Bedurke, T. Klamroth, and P. Saalfrank, Phys. Chem. Chem. Phys. **23**, 13544 (2021).
[51] E. Coccia, B. Mussard, M. Labeye, J. Caillat, R. Taïeb, J. Toulouse, and E. Luppi, Int. J. Quantum Chem. **116**, 1120 (2016).
[52] E. Coccia and E. Luppi, Theor. Chem. Acc. **135**, 43 (2016).
[53] E. Luppi and M. Head-Gordon, Mol. Phys. **110**, 909 (2012).
[54] E. Luppi and M. Head-Gordon, J. Chem. Phys. **139**, 164121 (2013).
[55] M. Labeye, F. Zapata, E. Coccia, V. Véniard, J. Toulouse, J. Caillat, R. Taïeb, and E. Luppi, J. Chem. Theory Comput. **14**, 5846 (2018).
[56] E. Coccia and E. Luppi, Theor. Chem. Acc. **138**, 96 (2019).
[57] A. F. White, C. J. Heide, P. Saalfrank, M. Head-Gordon, and E. Luppi, Mol. Phys. **114**, 947 (2016).
[58] E. Coccia, R. Assaraf, E. Luppi, and J. Toulouse, J. Chem. Phys. **147**, 014106 (2017).
[59] J. A. Sonk, M. Caricato, and H. B. Schlegel, J. Phys. Chem. A **115**, 4678 (2011).
[60] J. A. Sonk and H. B. Schlegel, J. Phys. Chem. A **115**, 11832 (2011).
[61] H. B. Schlegel, S. M. Smith, and X. Li, J. Chem. Phys. **126**, 244110 (2007).
[62] N. Tancogne-Dejean, M. J. T. Oliveira, X. Andrade, H. Appel, C. H. Borca, G. Le Breton, F. Buchholz, A. Castro, S. Corni, A. A. Correa *et al.*, J. Chem. Phys. **152**, 124119 (2020).
[63] T. P. Rossi, M. Kuisma, M. J. Puska, R. M. Nieminen, and P. Erhart, J. Chem. Theory Comput. **13**, 4779 (2017).
[64] S. A. Fischer, C. J. Cramer, and N. Govind, J. Chem. Theory Comput. **11**, 4294 (2015).
[65] P. Hoerner, M. K. Lee, and H. B. Schlegel, J. Chem. Phys. **151**, 054102 (2019).
[66] R. Rüger, M. Franchini, T. Trnka, A. Yakovlev, E. van Lenthe, P. Philipsen, T. van Vuren, B. Klumpers, and T. Soini, AMS 2022.1, SCM, Theoretical Chemistry, Vrije Universiteit, Amsterdam, The Netherlands, 2022, http://www.scm.com.
[67] R. G. Parr and W. Yang, *Density-Functional Theory of Atoms and Molecules* (Oxford University Press, 1989), Vol. 1, p. 1989.
[68] G. te Velde, F. M. Bickelhaupt, E. J. Baerends, C. Fonseca Guerra, S. J. A. van Gisbergen, J. G. Snijders, and T. Ziegler, J. Comput. Chem. **22**, 931 (2001).
[69] A. D. Becke, J. Chem. Phys. **98**, 5648 (1993).
[70] C. Meinert, A. D. Garcia, J. Topin, N. C. Jones, M. Diekmann, R. Berger, L. Nahon, S. V. Hoffmann, and U. J. Meierhenrich, Nat. Commun. **13**, 502 (2022).
[71] M. E. Casida, *Recent Advances in Density Functional Methods: (Part I)* (World Scientific, 1995), pp. 155–192.
[72] T. Yanai, D. P. Tew, and N. C. Handy, Chem. Phys. Lett. **393**, 51 (2004).
[73] A. Kumar, S. E. Toal, D. DiGuiseppi, R. Schweitzer-Stenner, and B. M. Wong, J. Phys. Chem. B **124**, 2579 (2020).
[74] A. Klamt and G. Schüürmann, J. Chem. Soc., Perkin Trans. 2 **1993**, 799–805.
[75] M. Carnell, S. D. Peyerimhoff, A. Breest, K. H. Gödderz, P. Ochmann, and J. Hormes, Chem. Phys. Lett. **180**, 477 (1991).
[76] R. C. Fay and R. B. Von Dreele, J. Am. Chem. Soc. **93**, 4936 (1971).
[77] K. Hiramatsu and T. Nagata, J. Chem. Phys. **143**, 121102 (2015).
[78] V. Stadnytskyi, G. S. Orf, R. E. Blankenship, and S. Savikhin, Rev. Sci. Instrum. **89**, 033104 (2018).
[79] M. Oppermann, B. Bauer, T. Rossi, F. Zinna, J. Helbing, J. Lacour, and M. Chergui, Optica **6**, 56 (2019).
[80] M. Kuronuma, T. Sato, Y. Araki, T. Mori, S. Sakamoto, Y. Inoue, O. Ito, and T. Wada, Chem. Lett. **48**, 357 (2019).
[81] M. Schmid, L. Martinez-Fernandez, D. Markovitsi, F. Santoro, F. Hache, R. Improta, and P. Changenet, J. Phys. Chem. Lett. **10**, 4089 (2019).
[82] A. Sharma, S. Athanasopoulos, E. Kumarasamy, C. Phansa, A. Asadpoordarvish, R. P. Sabatini, R. Pandya, K. R. Parenti, S. N. Sanders, D. R. McCamey *et al.*, J. Phys. Chem. A **125**, 7226 (2021).
[83] M. Cao, S. Q. Newton, J. Pranata, and L. Schäfer, J. Mol. Struct.: THEOCHEM **332**, 251 (1995).
[84] S. Blanco, A. Lesarri, J. C. López, and J. L. Alonso, J. Am. Chem. Soc. **126**, 11675 (2004).
[85] J. Fan and T. Ziegler, Inorg. Chem. **47**, 4762 (2008).